16th Inter. Cong. on High Speed Photography and Photonics
M. Andre and M. Hugonschmidt, eds., Proc. SPIE 491, pp. 180-187 (1984)

Tomographic reconstruction of axially symmetric objects from a single radiograph

Kenneth M. Hanson

Hydrodynamics Group, Los Alamos National Laboratory
Mail Stop P940, Los Alamos, New Mexico 87545 USA

Abstract

In 1826 Abel presented the method of obtaining the profile of a circularly symmetric 2-D object from its projection. It is shown that the extension of Abel inversion, the reconstruction of a 3-D axially symmetric object from a single radiograph, offers significant benefits as an image analysis tool. These benefits include improved delineation of material boundaries, enhanced display of minor deviations from axial symmetry, as produced by defects, and accurate estimation of the linear attenuation coefficients of the materials. Frequently this technique allows observation of features in the object that are too subtle to be seen in the original radiograph.

Introduction

The reconstruction of a two-dimensional object with circular symmetry from a single projection was determined by Abel in 1826.[1] It is possible to extend this 2-D analysis to reconstruct the cross section of a three-dimensional, axially symmetric object from a single radiograph taken with the radiographic axis perpendicular to the symmetry axis, as depicted in Fig. 1. This method has been applied to many problems in many different fields in the past, including two recent applications to nondestructive testing at Los Alamos.[2,3] In industrial radiography, where many objects have nearly circular symmetry, such an approach offers significant benefits as an image analysis tool. These benefits include improved delineation of material boundaries, enhanced display of deviations from axial symmetry, for example, defects, and estimation of the radial dependence of the attenuation coefficients of the materials. It is often possible to observe in the reconstruction subtle features of the

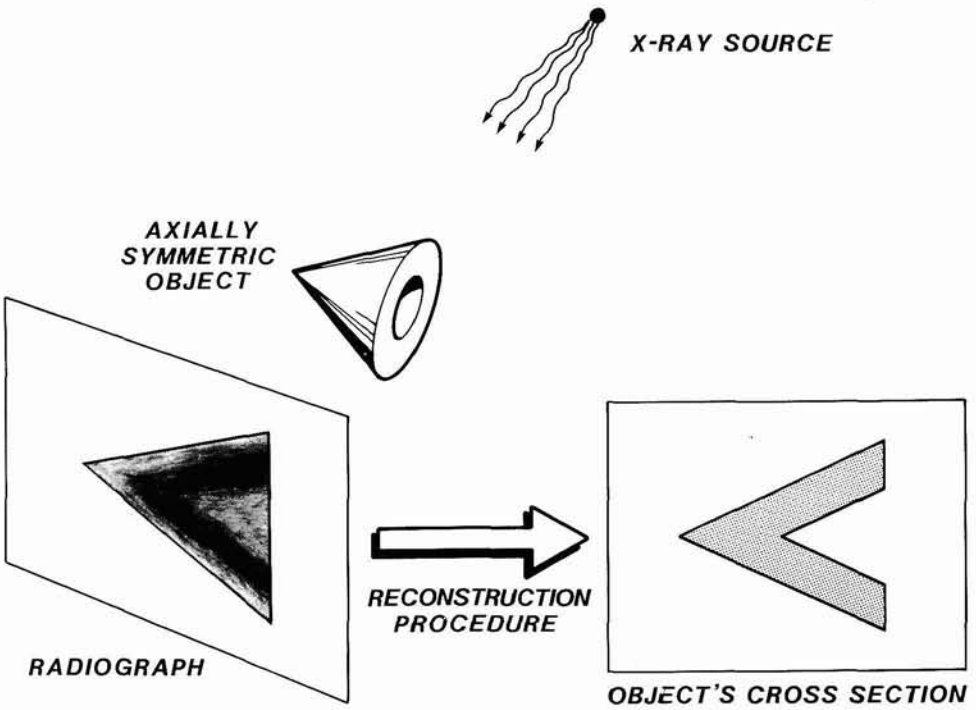

Fig. 1. Overview of tomographic method. An axially symmetric object is radiographed with the radiographic axis perpendicular to the axis of symmetry. The reconstruction procedure produces the cross section of the object.

object that are unobservable in the original radiograph. The improvements brought about by the tomographic method are due to the effective removal of overlying material from the radiograph and the resultant increase in contrast with which it is possible to display the reconstruction. The utility of the tomographic analysis is demonstrated by the reconstruction of the cross section of a solid metal object with axial symmetry from a single radiograph.

Method

Suppose that f(x,y) is an unknown function of the two spatial variables, x and y, and that it possesses a compact region of support, that is, f is zero outside of a local region. It was shown by Radon[4] nearly seventy years ago that it is possible to determine f from a set of line integrals

$$p(R,\theta) = \int_L f(x,y)\, ds \qquad (1)$$

where the line integral is taken along the straight line L, L being specified by its distance to the origin R and its angle with the x-axis θ, provided that p is given for all lines that intersect the region of support of f. The set of line integrals with the same angle θ is called the projection at that angle. The possibility that f may be reconstructed from projections has been put to use in the relatively new technique called computed tomography (CT) or computerized axially tomography (CAT) scanning. The striking success of this revolutionary technique in medical radiography is now legend.

In practice, the tomographic reconstruction of an arbitrary 2-D object normally requires projection measurements at a large number of angles. However, when the function possesses circular symmetry, only one projection is needed as every projection is the same. Thus if f is known not to depend upon θ, Eq. (1) may be rewritten as

$$p(R) = 2 \int_R^\infty \frac{f(r)\, r\, dr}{\sqrt{r^2 - R^2}} \qquad (2)$$

where f and p are now functions only of the radius R. This is recognized as the Abel transform for which Abel[1] derived the inverse. More recent work on the numerical evaluation of the Abel inverse include references 5-8. In the present work, the Abel inversion is accomplished using a simplified version of the well-known filtered backprojection algorithm[9,10] that can be used to solve the more general problem of reconstruction of an arbitrary 2-D object from a large number of 1-D projections covering 180 degrees. To illustrate this, consider Fig. 2a, which shows a circularly symmetric 2-D function. The projection of this function, Fig. 3a, is the same at all angles. Use of the filtered backprojection algorithm with identical projections at 180 angles yields the complete 2-D reconstruction shown in Fig. 2b. In this algorithm, the result of filtering the projection by $|w| \exp(-c|w|^2)$, where w is the spatial frequency, is backprojected upon the reconstruction grid of pixels. Here, c is chosen such that the exponential has a value of 1/2 at half the Nyquist frequency ($f_N = 1/(2\ \Delta R)$), where ΔR is the spacing between projection samples. The exponential is employed to reduce the ringing in the reconstruction that would otherwise be present if the ramp $|w|$ were not smoothly attenuated at high frequencies. Because the full 2-D reconstruction, Fig. 2b, has circular symmetry, it may be summarized by its radial dependence, shown in Fig. 3b. Fig. 3b is a good representation of the radial dependence of the original two annuli showing only a slight loss in spatial resolution owing to the limited number of projection samples (128) and the use of the exponential apodization function in the filter. In the present version of the filtered backprojection algorithm, the filtering is done only once and the backprojection is calculated for only the single line of the reconstruction that passes through the origin. The backprojection operation is carried out for a sufficiently large number of angles, typically 1.5 times the number of samples in the projection. Incidentally, the duplicated projections are assumed to span 180° with the projection rays parallel to the reconstruction line at 0° and 180°. Therefore the major contribution to the reconstruction on each side of the rotation axis comes predominately from the corresponding side of the projection. From an alternative viewpoint, Abel inversion may be thought of as a deconvolution procedure since the given projection is the convolution of the original function with a known, nonstationary point spread function.

Suppose that a 3-D object is radiographed with an essentially monoenergetic x-ray source. If the x rays are detected with a direct-recording film, the optical density of the developed film is proportional to the x-ray intensity. The film's optical density at the intersection of a line L, which originates at the point source, with the film plane is given by

$$D_L = D_0 + D_1 \exp(-p_L) \qquad (3)$$

where the pathlength p_L is the line integral along line L of the object's linear attenuation coefficient distribution $\mu(x,y,z)$, evaluated at the energy of the x rays used,

$$p_L = \int_L \mu(x,y,z)\, ds. \qquad (4)$$

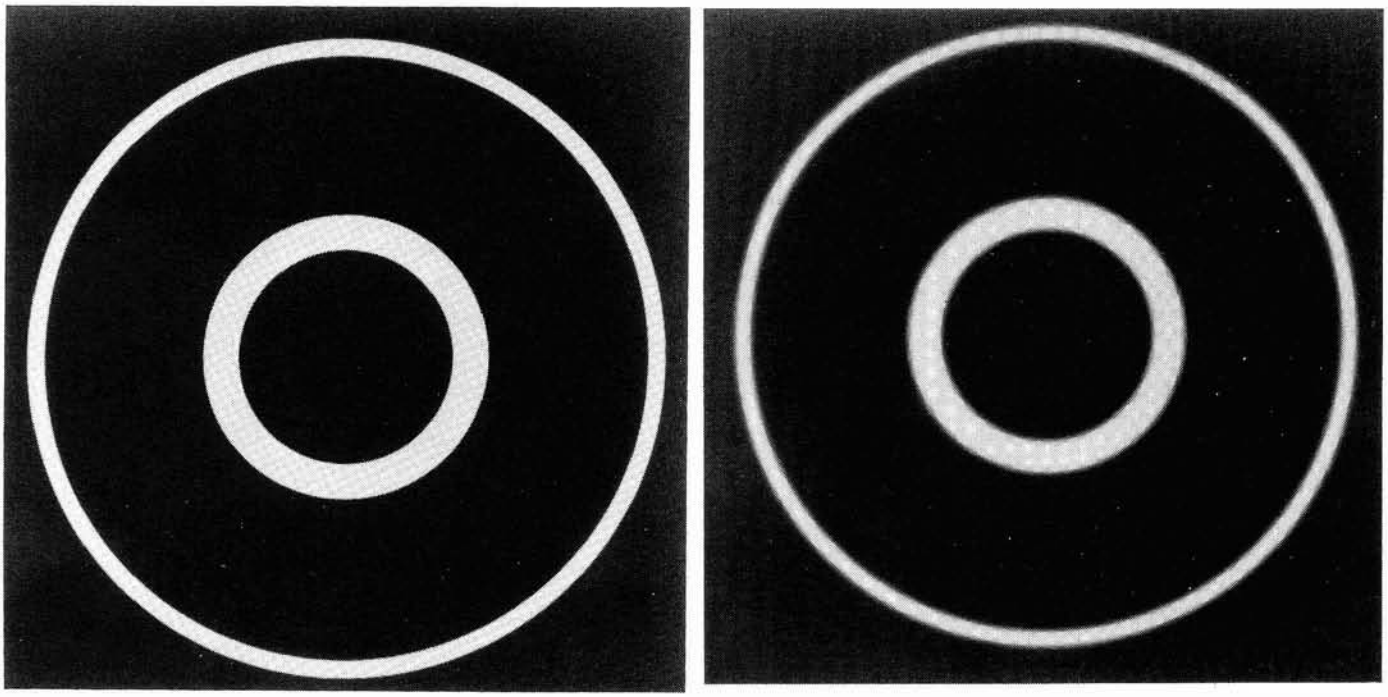

Fig. 2. a) A 2-D function with circular symmetry consisting of two annuli. b) The reconstruction of a) obtained using 180 parallel projections, each consisting of 128 samples.

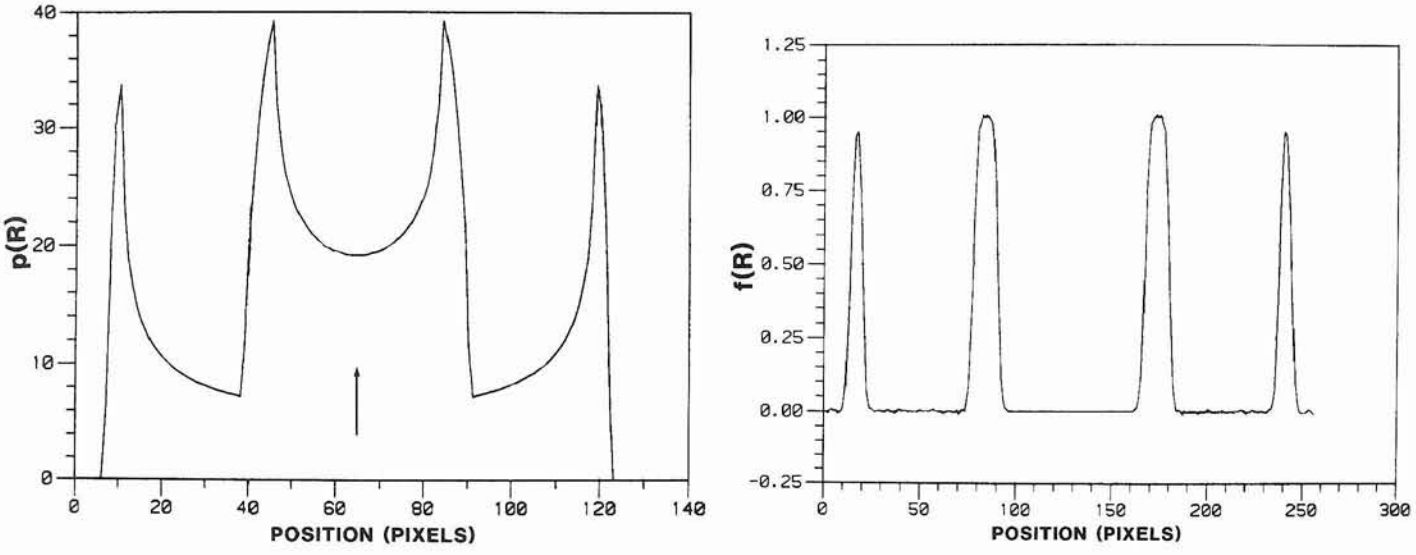

Fig. 3. a) The parallel projection of the function shown in Fig. 2a. b) The radial dependence of the 2-D reconstruction of the function shown in Fig. 2b done on a finer grid. The calculation of b) from a) is the Abel inversion process.

In Eq. (3) D_0 is the background density of the film at that point, which includes the fog value of the film and any contribution from scattered radiation. D_1 is the net density (above D_0) that would be obtained in the absence of the object. Thus it is seen that the projections needed as input for tomographic reconstruction, Eq. (1), may be obtained from radiographic measurements. Inversion of Eq. (3) yields the pathlength in terms of measured film density D_L

$$p_L = -\ln\left(\frac{D_L - D_0}{D_1}\right) \tag{5}$$

From the previous discussion, it is seen that tomographic reconstruction based upon projections obtained in this way will yield the linear attenuation coefficient distribution of the object.

Now consider a 3-D object that possesses axial or rotational symmetry. In any plane that is perpendicular to the symmetry axis, the object's cross section has circular symmetry. If the object is radiographed with a set of parallel x-ray beams, all of which lie in such a plane, equivalent to a point source placed infinitely far from the object, the pathlengths obtained from applying Eq. (5) will correspond precisely to those considered in the 2-D example above. Thus the radial distribution of that cross section can be reconstructed using the same technique. A line-by-line analysis carried out in this way on each line of the radiograph that is perpendicular to the symmetry axis yields the complete radial distribution of μ for the object. This line-by-line analysis is legitimate because the contributions to each line come from one and only one cross-sectional plane through the object and each cross section has circular symmetry. In practice, the x-ray source cannot be placed infinitely far from the object. Indeed, it is often placed very close. In this case, the line-by-line analysis is not strictly valid as the contributions to each line of the radiograph, with the possible exception of a single line, come from neighboring cross sections. Owing to its simplicity, the line-by-line method is employed in the present analysis even though it may not be exactly correct. The consequences of this approximation will be explored in the Discussion section.

Results

An axially symmetric test object was constructed in order to illustrate the usefulness of the tomographic analysis technique. The object is a 70-mm-long right circular steel cylinder, 120 mm in diameter, with a 45° cone removed from one end to a depth of 40 mm. 2-mm-square grooves were machined on the flat face as well as on the inside of the cone at radii of 10, 20, 30, and 40 mm. A 2-mm-diameter, 2-mm-deep hole was also drilled into the center of the flat face. This object was radiographed with a 120 Ci Co^{60} source for 15 minutes using Kodak AA film placed in close contact with 0.25-mm-thick lead screens, front and back. The source diameter was about 1.5 mm. In order to closely approximate the parallel beam geometry that is assumed by the reconstruction procedure, the source was placed 4.6 m from the object, which was in close proximity to the film. The film was scanned on a Perkin-Elmer/PDS-2020 microdensitometer to produce a digital image that was 220 by 220 pixels in size with pixel spacing of 0.6 mm. Fig. 4a shows the optical density measured along a single line from the middle of the radiograph, displayed in Fig. 5a. It is seen that the machined-measured density varies between roughly 0.5 and 3.5. In terms of diffuse density units, these values correspond to about 0.3 and 2.3. The latter corresponds to the total density produced by the unattenuated x-ray beam.

Figure 4 illustrates the tomographic analysis procedure that is done on each line of the digitized image. The value of $D_0 + D_1$ is seen to be 3.5 from Fig. 4a. The value of 0.49 is chosen for D_0 to produce a reconstruction that has a value of about zero on the inside of the cone. Fig. 4b displays the pathlength integral obtained from Fig. 4a using Eq. (5). It is seen that the small noise level in the film density is considerably amplified, particularly so as the density approaches the background level D_0. Indeed, Eq. (5) indicates that when D_L is less than D_0, the pathlength cannot be calculated. Such a situation is simply unphysical. This points out the nonlinear nature of Eq. (5) that can result in substantial enhancement of the noise for thick objects. Before reconstruction, the pathlength is corrected for a slowly varying D_1 by subtracting off a background, which is linearly interpolated between the two end segments of the curve, known to lie outside the object. Furthermore, the data in the end segments are smoothly tapered to zero using a Hanning function, $0.5(1 + \cos(x))$. This is to meet the requirement of the filtered backprojection algorithm that the input projections fully encompass the object. The reconstruction of the radial dependence of the attenuation coefficient, using the procedure described above, results in Fig. 4c. This reconstruction depicts the cross section of an annulus of constant attenuation coefficient fairly well. The mean value of μ obtained for the steel shell agrees with the tabulated value of the attenuation coefficients for iron at 1.25 MeV, namely 0.042 mm^{-1}.[11] The noise in the pathlength data has been further amplified. There is severe enhancement of the noise near the axis of symmetry (at 112 pixels) that

arises from a nearly singular condition in the reconstruction procedure there. This amounts to the physical statement that as a ring of material with constant thickness decreases in diameter, it produces a smaller and smaller optical density signal, making it increasingly difficult to observe in the presence of nearly constant film-density noise.

When the above analysis is performed on each line of the radiograph, Fig. 5a, and the reconstructed radial profiles are combined to form an image, Fig. 5b results. The entire computation time to obtain this result was 1.4 min of CPU time on a CDC7600. This reconstruction closely resembles the cross section of the object itself. Furthermore, the grooves, which were very difficult to observe in the original radiograph, are now easily seen. In the original radiograph the grooves on the flat face of the cylinder produced fluctuations in diffuse optical density of from 0.016 for the 10-mm-radius groove to 0.057 for the 40-mm one. These correspond to contrasts in light luminance of from 4% to 14%. While a 4% contrast is visually observable under the best of viewing conditions,[12] it is essentially impossible to observe in the original radiograph, where the edge of the cylinder creates a rapidly falling luminance profile. On the other hand, this groove is readily seen in the reconstruction. The tomographic reconstruction procedure has redisplayed the data in such a way that it is the noise in the original radiograph that ultimately limits one's ability to derive information from it. This is the primary goal of image processing! The application of the tomographic analysis to the radiographs of other test objects has shown that it greatly enhances the visualization of minor defects in the objects and that these defects remain localized in the reconstruction. It is interesting to note that the noise level in the reconstruction image, Fig. 5b, seems much more tolerable than in the single line, Fig. 4c. Not only does the 2-D grey-scale image display more information than individual line graphs, but it provides a better interface to human observers. The eye-brain system is used to dealing with 2-D scenes, which the image Fig. 5b resembles. We humans are much better at pattern recognition when presented with such a 2-D image than when confronted with a 1-D graph as in Fig. 4c.

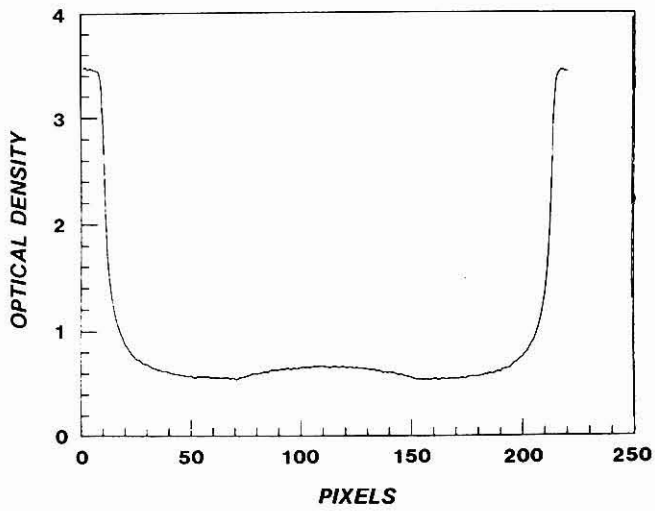

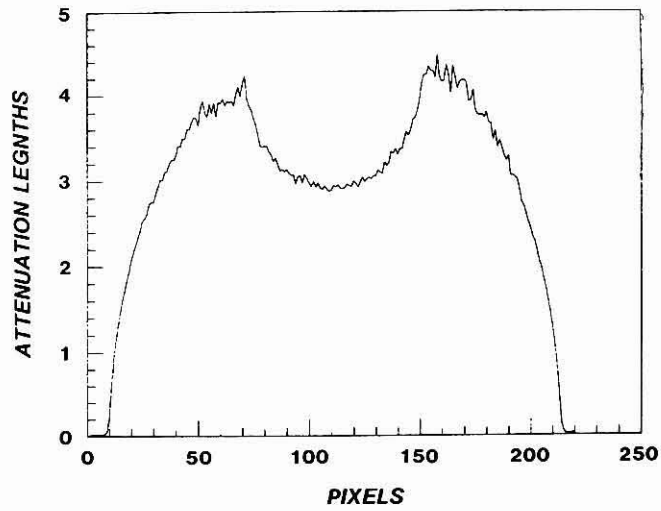

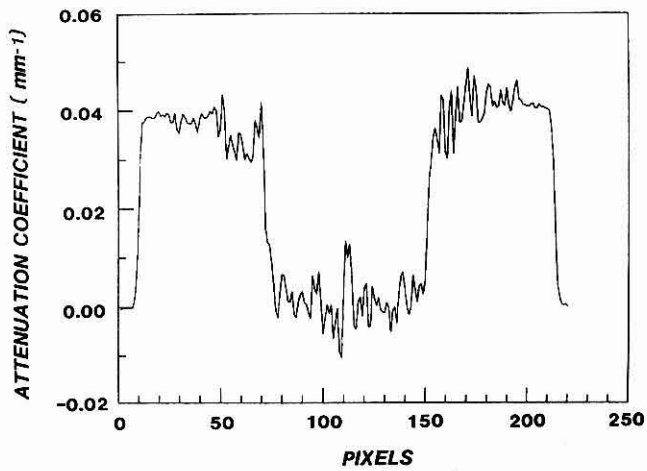

Fig. 4. a) The optical density along a horizontal line from the radiograph shown in Fig. 5a as read by a microdensitometer. The horizontal position is measured in pixel widths (= 0.6 mm). b) The projected path length obtained from these optical density data using Eq. (5). c) The radial dependence of the object's linear attenuation coefficient distribution reconstructed from Fig. 4b assuming axial symmetry for the object.

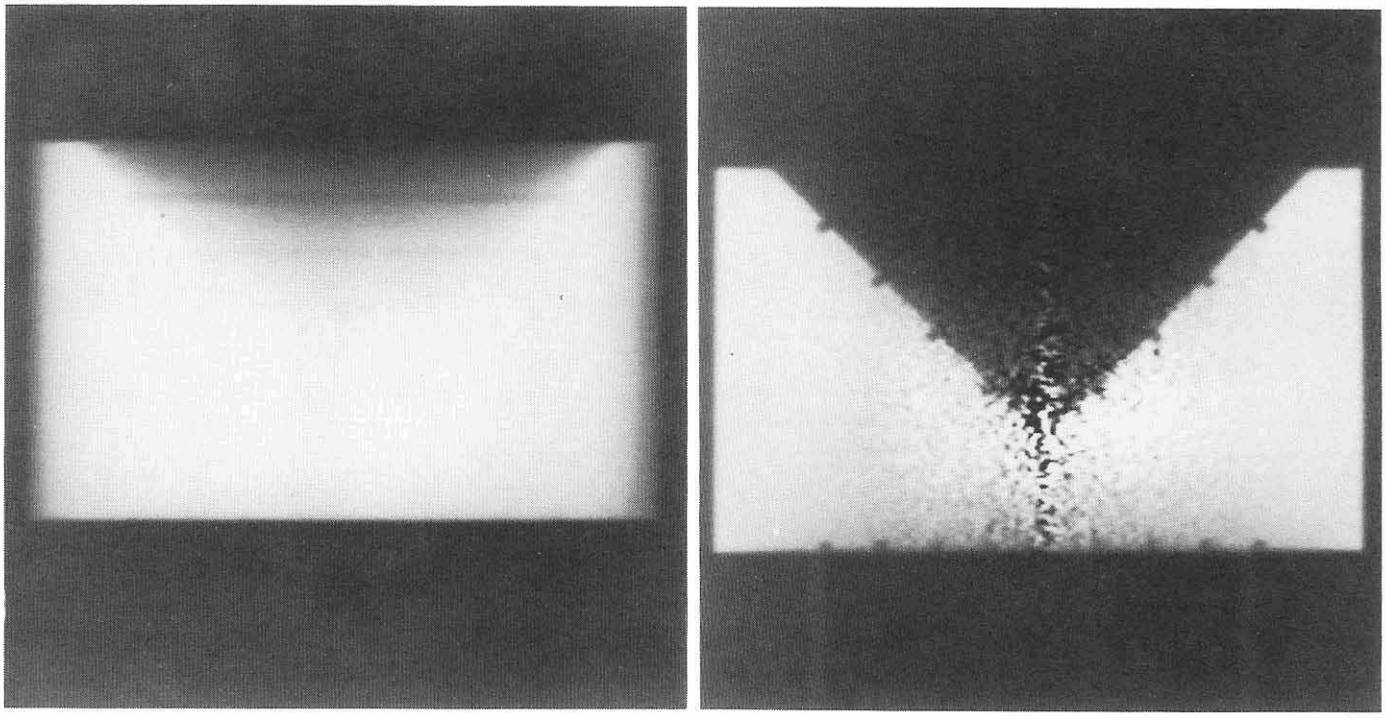

Fig. 5. a) Radiograph of an axially symmetric steel object taken with a Co^{60} source. The AA film was sandwiched between two 0.25-mm-thick lead screens. b) Display of the reconstruction of the object's cross section derived from Fig. 5a. The 2mm × 2mm grooves machined in the inside cone and on the end surface are readily apparent. These grooves were almost invisible in the original radiograph.

It is observed that the reconstruction values are slightly elevated on the right side of the middle of the object and that the noise levels are worse there. This is probably caused by a small decrease in the scattered radiation intensity in that region. The highly nonlinear behavior of Eq. (5) near $D = D_0$ makes the reconstruction very sensitive to the choice for D_0. A decrease of only 0.02 density units in D_0 is sufficient to remove the observed rise in reconstruction value in this region. This points out the need to know D_0 very accurately to avoid making serious systematic errors in the reconstruction.

Discussion

The effect of having nonparallel x rays in practical radiographic setups was discussed earlier. To demonstrate the effect of this, the same test object was radiographed with the axis of symmetry tilted away from the film by 7°, Fig. 6a. Now all the circular grooves in the object appear as ellipses instead of lines. The grooves on the flat end of the cylinder are much more visible than before because they are being seen through less material. When the tomographic analysis is performed on this radiograph in exactly the same way as before, the reconstruction shown in Fig. 6b is obtained. While not as representative of the cross section of the object as Fig. 5b, this reconstruction displays well most of the features of the object and can be readily interpreted. The grooves are reconstructed as ellipses because no account of the tilt of the axis of symmetry has been taken. In order to include the tilt or the lack of parallel rays in the radiographic geometry in the reconstruction procedure, the line-by-line mode of analysis would have to be abandoned. This would undoubtedly lead to a more complicated reconstruction algorithm and longer computing times, but the improvement may merit these costs.

The uncontrolled growth of noise in the reconstructions, especially near the axis of symmetry, poses a problem because the eye-brain system cannot successfully average image noise when it gets too large. What seems to be called for is a variable amount of smoothing of the input data. One method to control the noise in the reconstruction appears to be that of nonlinear maximum *a posteriori* probability (MAP) restoration, introduced to image processing by Hunt.[13] The application of this iterative approach to the problem of reconstruction of axially symmetric objects will be reported elsewhere.[14] The MAP approach has also proven to be a valuable tool for incorporation of *a priori* knowledge in tomographic reconstruction from a limited data set.[15]

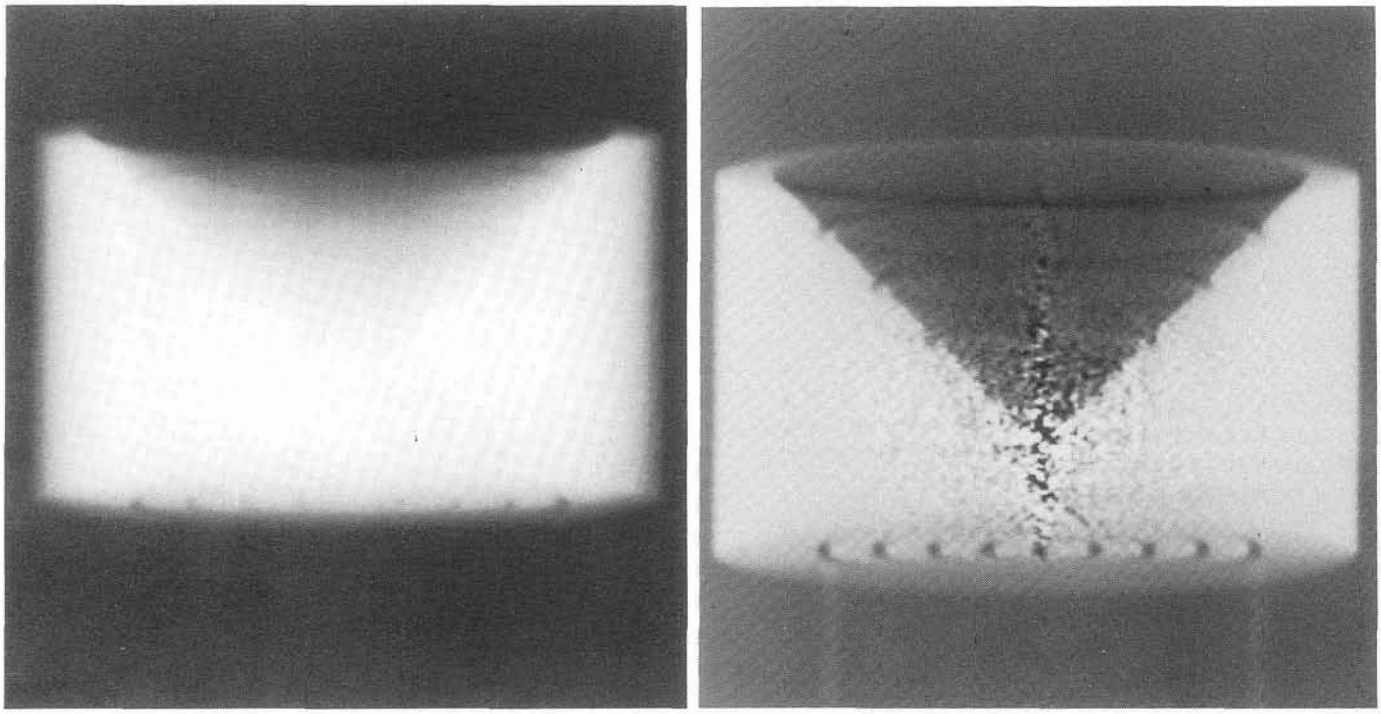

Fig. 6. a) Radiograph of the same object with a 7° tilt of the object's axis of symmetry. b) The reconstruction still shows many of the object's features even though the reconstruction procedure does not take the tilt into account.

In the preceding analysis, D_0 and D_1 are assumed to be constant throughout the radiograph. This gives rise to a nonuniform reconstruction of the steel's attenuation coefficient. An improvement in the tomographic procedure would allow these two parameters to vary. This would be easy to implement in the computer code. However, the problem then becomes one of determining these parameters everywhere, which is not so trivial. An interesting approach to solving this would be to parametrize these functions using a few parameters for each and include the estimation of these parameters in the reconstruction procedure. This could only be accomplished if some prior information about the object or the reconstruction, such as positivity of the reconstruction, is employed. One last difficulty in the tomographic analysis presented here is the assumption of a monochromatic source. Polychromatic x-ray sources are widely used. The attenuation law for these is not as simple as given in Eqs. (3) and (4). The problem is exacerbated by the possible presence of many, widely different kinds of material that might be present in industrial radiographic investigations. While the slight polychromatic (beam hardening) effects present in medical CT scanners have been successfully eliminated,[16] the general problem in industrial radiography remains a formidable one.

Acknowledgments

Thanks are due George Brooks for providing the radiographs used in the examples. This work was supported by the U. S. Department of Energy under contract number W-7405-ENG-36.

References

1. Abel, N. H., "Résolution d'un Probléme de Mecanique", J. Reine u. Angew. Math., vol. 1, pp. 153-157. 1826.
2. Fugelso, E., "Material Density Measurements from Dynamic Flash X-Ray Radiographs Using Axisymmetric Tomography," Los Alamos National Laboratory report LA-8785-MS 1981.
3. Berzins, G. J., McKinnon, G. C., Bates, R. H. T., and Lumpkin, A. H., "Application of Computed Tomography Techniques to Pinhole Images of Nuclear-Reactor Test Fuel Rods," Nucl. Sci. Eng., vol. 77, pp. 493-495. 1981.
4. Radon, J., "On the Determination of Functions from their Integrals along Certain Manifolds," Math.-Phys. Klasse, vol. 69, pp. 262-277. 1917.
5. Porter, R. W., "Numerical Solution for Local Emission Coefficients in Axisymmetric Self-Absorbed Sources," SIAM Rev., vol. 6, pp. 228-242. 1964.

6. Corti, S., "The Problem of Abel Inversion in the Determination of Plasma Density from Phase Measurements," Let. Nuovo Cim., vol. 29, pp. 25-32. 1980.
7. Deutsch, M., and Beniaminy, I., "Derivative-free Inversion of Abel's Integral Equation," Appl. Phys. Lett., vol. 41, pp. 27-28. 1982.
8. Deutsch, M., and Beniaminy, I., "Inversion of Abel's Integral Equation for Experimental Data," Appl. Phys. Lett., vol. 54, pp. 137-143. 1982.
9. Bracewell, R. N., and Riddle, A. C., "Inversion of Fan-Beam Scans in Radio Astronomy," Astrophys. Jour., vol. 150, pp. 427-434. 1967.
10. Shepp, L. A., and Logan, B. F., IEEE Trans. Nucl. Sci., vol. NS-21, pp. 21-43. 1974.
11. Grodstein, G. W., "X-Ray Attenuation Coefficients from 10 kev to 100 MeV," National Bureau of Standards Circular 583. 1957.
12. Burgess, A. E., Humphrey, K., and Wagner, R. F., "Detection of Bars and Discs in Quantum Noise," Proc. SPIE, vol. 173, pp. 34-40. 1979.
13. Hunt, B. R., "Bayesian Methods in Nonlinear Digital Image Restoration," IEEE Trans. Comp., vol. 3, pp. 219-229. 1977.
14. Hanson, K. M., "A Bayesian Approach to Nonlinear Inversion: Abel Inversion from X-Ray Attenuation Data," Proc. Fourth Workshop on Maximum Entropy and Bayesian Methods, Justice, J. H., ed., Calgary, August 6-8, 1984. (In press).
15. Hanson, K. M., and Wecksung, G. W., "Bayesian Approach to Limited-Angle Reconstruction in Computed Tomography," J. Opt. Soc. Amer., vol. 73, pp. 1501-1509. 1983.
16. Joseph, P. M., and Spital, R. D., "A Method for Correcting Bone Induced Artifacts in Computed Tomography Scanners," J. Comput. Assist. Tomogr., vol. 2, pp. 100-108. 1978.